IONOSPHERIC ALFVÉN RESONATOR CONTROL OVER THE FREQUENCY-VARIABLE PC1 EVENT IN FINLAND ON MAY 14, 1997

K. PRIKNER

Geophysical Institute, Academy of Sciences of the Czech Republic, Prague, Czech Republic[1]

K. MURSULA, J. KANGAS

Department of Physical Sciences, University of Oulu, Oulu, Finland[2]

F. Z. FEYGIN

United Institute of Physics of the Earth, Russian Academy of Sciences, Moscow, Russia[3]

Summary: *The ionospheric Alfvén resonator (IAR) control mechanism over the EMIC wave transmission to the ground is demonstrated on a selected long-term frequency-variable subauroral Pc1 event. The proper ionospheric plasma data obtained from EISCAT were accessible in a wide altitude range. Applying the numerical method of simulation of a realistic inhomogeneous IAR, the problem of appearance and disappearance of the ground Pc1 signal record was clarified on the basis of coincidence between the EMIC wave frequency spectrum and the IAR fundamental frequency peak (the frequency window). A shift of the signal source field line to lower latitudes during the development of the disturbance was noticed, and the signal frequency variation on the ground was modelled in the nonstationary IAR. Variation of the IAR altitude structure in the fundamental frequency was illustrated on altitude profiles of the normalized wave magnetic field amplitude in the horizontal and vertical components. Particular conditions of $L_{||}$- and $R_{||}$-wave mode incidence were assumed. The electron density vertical profile of IAR determines the effective resonator dimensions. In this way the IAR fundamental frequency window controls the signal within the ionosphere and on the ground.*

Keywords: Pc1 pulsations, Pc1 pearls, ionospheric Alfvén resonator, resonator response, fundamental frequency window, EISCAT measurements.

1. INTRODUCTION

The idea of the ionospheric Alfvén resonator (IAR) was first suggested by *Polyakov (1976)*, and later developed by *Polyakov and Rapoport (1981)*. The ionosphere up to altitudes of around 3000 km operates as an inhomogeneous Alfvén resonator for EMIC waves of frequencies 0.1 – 5 Hz propagating along magnetic field lines from the magnetosphere to the ground surface.

1 Address: Boční II, 141 31 Praha 4 – Spořilov, Czech Republic (e-mail: KPR@ig.cas.cz)

2 Address: P.O. Box 3000, FIN-90571 Oulu, Finland
(e-mail: Kalevi.Mursula@oulu.fi; Jorma.Kangas@sgo.fi)

3 Address: Bolshaya Gruzinskaya 10, 123810 Moscow, Russia
(e-mail: Feygin@uipe-ras.scgis.ru)

Simultaneously the ionospheric layer centered on the F layer density maximum can operate as a horizontal ionospheric waveduct (HIW) for magnetosonic waves of frequencies 0.2 – 5 Hz (*Greifinger and Greifinger, 1968; Altman and Fijalkow, 1980; Fujita, 1987; Lysak, 1999*).

The close connection between Pc1 and the fundamental resonance frequency of IAR has been studied in a series of papers (e.g., *Demekhov et al., 1994*), i.e. there is a close relation to the eigenfrequency of the resonator (*Belyaev et al., 1990; Lysak, 1991, 1993*). Also a close connection to the IAR fundamental frequency has been reported for subauroral IPDP events in the companion papers by *Mursula et al. (2000)* and *Prikner et al. (2000)*.

Both types of events, Pc1 and IPDP, should have a similar origin based on EMIC wave propagation through IAR under different disturbance conditions – Pc1 under relatively quiet, and IPDP under disturbed conditions in a nonstationary IAR during substorms. The IAR fundamental frequency spectral peak (*Prikner et al., 2000*) controls the position and width of the frequency window of the signal observed in the ionosphere and on the ground. Intensive signals can be observed on the ground only if the EMIC wave frequencies match the resonance peak window of IAR.

More questionable and speculative is the explanation of the fine pearl structure of Pc1 and IPDP types of signals, which are usually preserved within the IAR frequency window. Various mechanisms have to be taken into account (*Mursula et al., 2000*). In the first place it is the bouncing wave packet's frequency dispersion mechanism (*Jacobs and Watanabe, 1964; Obayashi, 1965*) related to the inward motion of the equatorial sources and to the decreasing repetition period of packets in IPDPs. This mechanism was criticized (*Erlandson et al., 1992, 1996; Fraser et al., 1996*). But the analysis of the repetition period in simultaneous ground and satellite observations of structured Pc1 pulsations once again points back to the problem of the wave packets bouncing between conjugated hemispheres. The mechanism of Pc1 pearl formation is discussed on the basis of the Alfvén sweep maser operation in *Trakhtengerts et al. (2000)*. The problem of wave bouncing at the maxima of the resonator reflection coefficient and the ground observation of pulsation signals at simulated IAR eigenfrequencies was discussed in *Demekhov and Trakhtengerts (2000)*.

The other mechanism suggested is non-bouncing Pc1 wave bursts modulated by long-period ULF waves (Pc3-5 pulsations – global modes) around the equatorial source region (*Mursula et al., 1997, 1999a; Rasinkangas and Mursula, 1998*). But this mechanism has difficulties with interpreting the alternative appearance of signals at conjugate points, and with the properties of their dispersion associated with signal propagation along the field line. The final conclusion still requires further experimental verification.

According to *Mursula et al. (2000)* the IPDP frequency increase has been interpreted on the basis of a non-stationary IAR mechanism. IPDP occurs simultaneously with the extension of the ionospheric trough region to lower latitudes in substorms (*Kleimenova et al., 1995*). It indicates non-stationary IAR plasma conditions during the event.

The sweeping out of the plasma from the higher ionosphere above the F-layer (possibly in connection with the feedback instability mechanism according to *Lysak, 1991*), and the plasma density increase in the lower E-F1 region during the substorm expansion phase (*Bauske et al., 1997*) cause the IAR frequency characteristics to vary and a gradual fundamental frequency increase. Simultaneous inward shifts of the equatorial EMIC wave sources, usually accompanied with a shift of the plasmapause to lower L-shells, provide a consecutive shift of the ground-observed IPDP disturbance to lower latitudes. A similar process in IAR will be demonstrated on a special selected frequency-variable Pc1 event recorded at a chain of Finnish observatories, using the simultaneous Scandinavian EISCAT incoherent scatter radar measurements of ionospheric plasma characteristics with the application of the numerical method simulating the IAR operation mechanism.

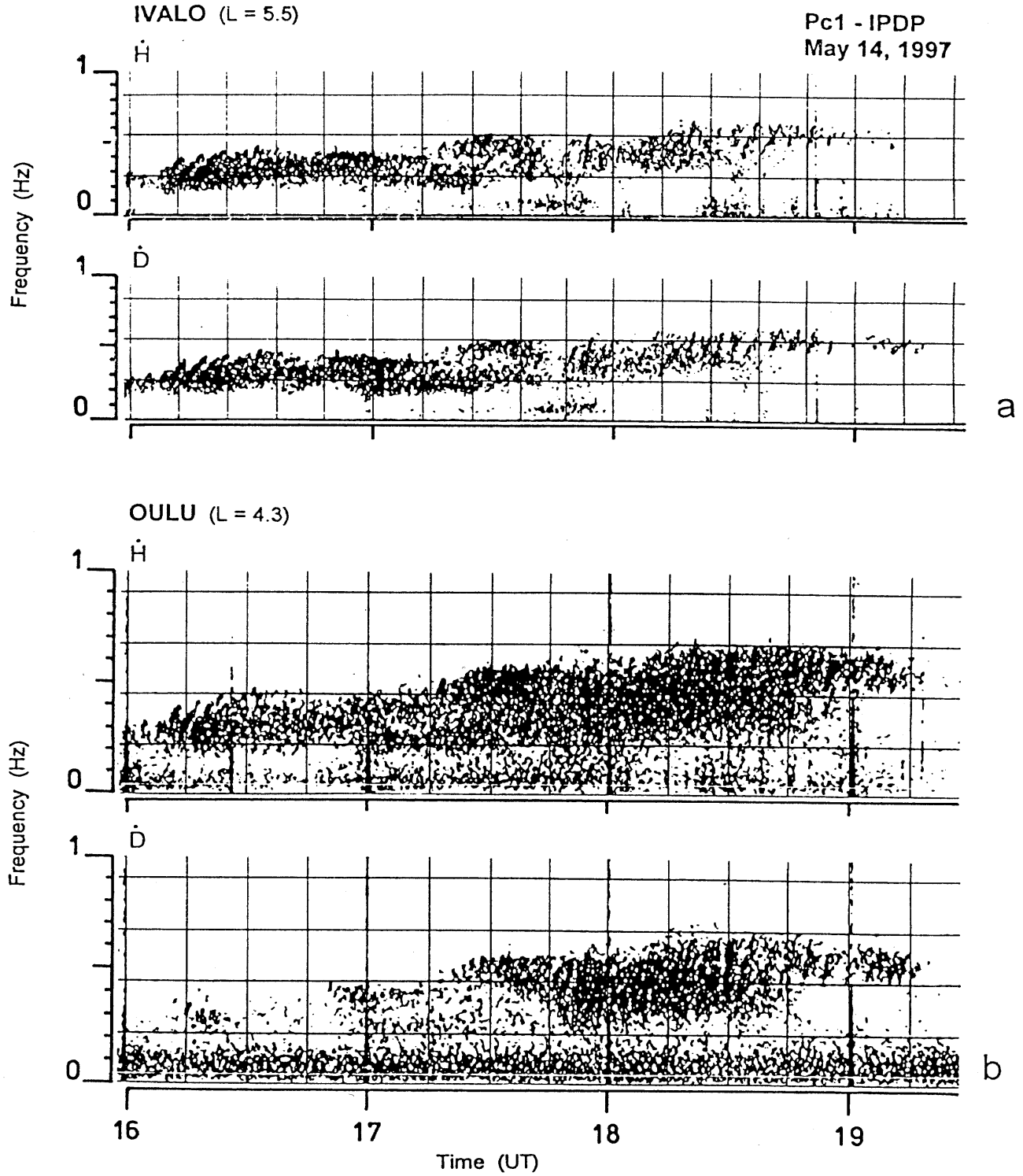

Fig. 1. The dynamic spectra of the ground signal records of the horizontal N-S (H) and azimuthal (D) magnetic field components at the Finnish stations of Ivalo (**a**) and Oulu (**b**).

2. OBSERVATIONS

The long-term frequency-variable Pc1 event was observed on May 14, 1997, within the interval 1600 UT to 1915 UT at the latitude chain of Finnish observatories (especially at Kilpisjarvi, Ivalo, Rovaniemi, and Oulu). During the development of the pulsation the disturbance showed a tendency to spread to lower latitudes. The intensive dynamic spectra of the search-coil magnetometer records from the two Finnish observatories, Ivalo ($L = 5.5$) and Oulu ($L = 4.3$) are shown in Fig. 1. They characterize the signal in two horizontal components, N-S (H), and azimuthal E-W (D).

The geographical and geomagnetic (Gustafsson's model) coordinates of both the observatories are: Ivalo, $\varphi = 68.55°$N, $\lambda = 27.28°$E, $\Phi = 64.9°$N, $\Lambda = 109.5°$E. Oulu, $\varphi = 65.05°$N, $\lambda = 25.54°$E, $\Phi = 61.5°$N, $\Lambda = 106.1°$E. The situation between the points, at which the signal was observed, is illustrated on the map of Scandinavia in Fig. 2. The geomagnetic field variation through the whole of 14 May is depicted in Fig. 3 for the intermediate auroral observatory Sodankylä ($L = 5.2$). The Pc1 interval of occurrence is marked by horizontal abscissae.

The detailed analysis of the dynamic spectra in Fig. 1 shows continuous structured pearl bands during almost the whole interval of the event at both the stations separated in latitude. The central frequency increased very slowly from about 0.31 Hz to 0.33 Hz within *the first interval* of the event, between 1600 UT and 1720 UT. The signal was of the Pc1 pearl structure type. Also one can see that the Ivalo station was very near the foot of the source magnetic field line with oscillations of comparable amplitudes in both the components, whilst at Oulu the azimuthal D-component was much less intensive, possibly due to the effect of the meridional compressional waveguide modes according to *Lysak (1999)*.

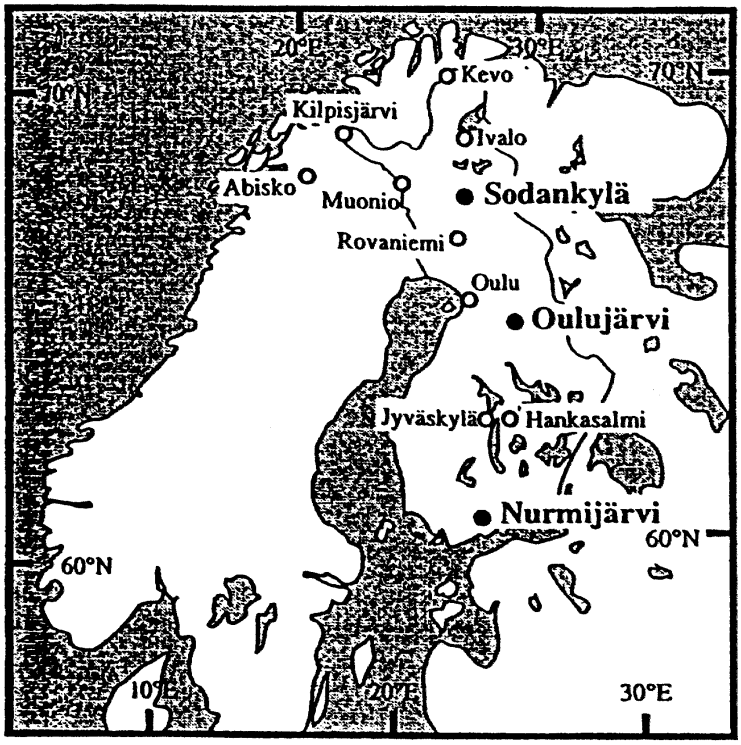

Fig. 2. A map of Scandinavia depicting the situation of the Pc1 event observation.

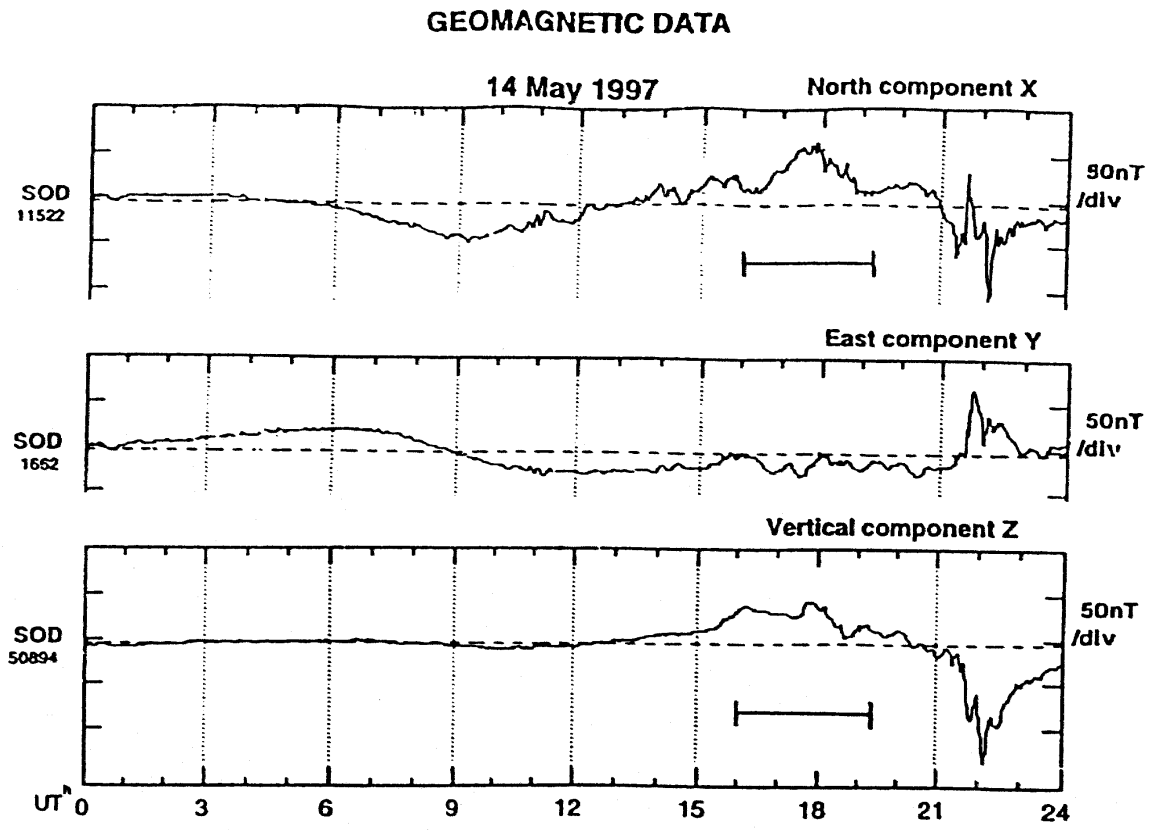

Fig. 3. A view of the external magnetic field variation at Sodankylä on 14 May 1997. The interval of the Pc1 event examined is the marked time interval.

The second interval of the event started at 1720 UT. The simultaneous increase of the mean frequency of the pulsation band was observed (Fig. 1) at Ivalo as well as at Oulu in both the components, H and D. Intensive oscillations of comparable amplitudes in both components at Oulu and a gradual decrease of amplitudes at Ivalo indicated a latitude shift of the feet of the source field lines towards Oulu, i.e. possible inward motion of the equatorial EMIC wave sources to lower L-shells. The mean frequency near ~0.5 Hz merged with the first harmonic resonant mode of the ionosphere waveguide cavity, according to *Lysak (1999)*. There exists a high possibility of horizontal propagation of generated compressional modes.

During the whole pulsation event the pearl structure was preserved. The pulsation bands became consecutively damped and disappeared completely after 1915 UT. The vertical plasma profile's variation of IAR and the variation of the IAR fundamental frequency* response on the ground during the whole pulsation event will be demonstrated later for the Ivalo region.

---

* By the term "fundamental frequency" of IAR we shall hereinafter understand the central frequency peak of the horizontal amplitude transmission coefficient through the IAR simulation domain (ionosphere layer up to an altitude of 1000 km), however, "eigenfrequencies" of a resonator are defined on the basis of the energy stored in the resonator, and may or may not exactly coincide with maxima of the transmission coefficient.

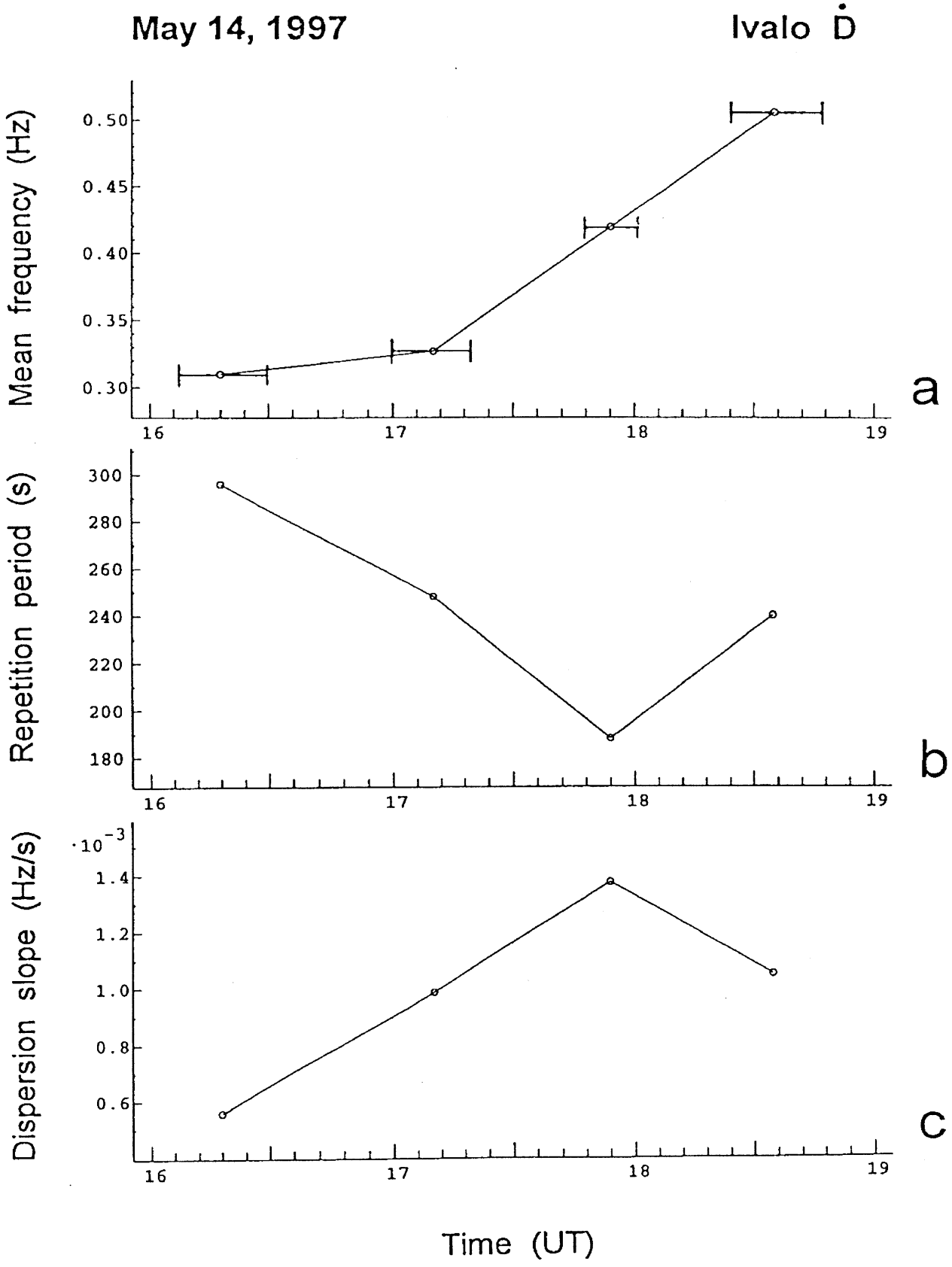

Fig. 4. The time variation of averaged values (averaging was carried out in the marked time intervals in part **a** of the figure) of the mean signal frequency in the D-component at Ivalo from Fig. 1a (**a**), the repetition periods (**b**), and the dispersion slope of particular pearl wave packets (**c**).

The direct treatment of the dynamic spectra of Ivalo and Oulu records (Fig. 1) with like amplitude sensitivities yielded some characteristics illustrating the event's development in the region. Within the first mentioned interval the frequency band limits were nearly the same both at Ivalo and Oulu. Ivalo seems to be the principal disturbance region. But within the second interval, after 1730 UT, the principal disturbance region seems to have shifted nearer to Oulu. The signal at Ivalo weakened (Fig. 1) and its band limits narrowed down with respect to the Oulu signal. This is an indication of a latitude shift of the disturbance with a possible inward motion of the equatorial EMIC wave sources. Also a gradual slow increase of the mean signal frequency is evident during the whole interval of the event.

The gradual systematic increase of the mean frequency, f_0 (Hz), determined from the Ivalo D-record at selected time intervals with a distinct pearl-packet structure is shown in Fig. 4a. The variation of the mean repetition period, τ (s), determined in the same time intervals marked in Fig. 4a, is depicted in Fig. 4b. A similar variation of the mean frequency dispersion slope of the individual pearl packets, S (Hz/s), is shown in Fig. 4c.

Four intervals of the packets' development have been selected in Fig. 4. Three groups of pearls existed till 1800 UT, and one later:

i) 1608 – 1630 UT, $f_0 = 0.31$ Hz, $\tau = 295$ s, $S = 5.6\times10^{-4}$ Hz/s. Then $f_0\tau = 91$, and $\tau/f_0 = 952$.

ii) 1700 – 1720 UT, $f_0 = 0.325$ Hz, $\tau = 248$ s, $S = 9.8\times10^{-4}$ Hz/s, and $f_0\tau = 81$, and $\tau/f_0 = 763$.

iii) 1748 – 1802 UT, $f_0 = 0.42$ Hz, $\tau = 189$ s, $S = 1.37\times10^{-3}$ Hz/s, and $f_0\tau = 79$, and $\tau/f_0 = 450$.

iv) 1825 – 1848 UT, $f_0 = 0.50$ Hz, $\tau = 240$ s, $S = 1.04\times10^{-3}$ Hz/s, and $f_0\tau = 120$, and $\tau/f_0 = 480$.

According to *Mursula et al. (1999b)* the ratio τ/f_0 can be used as the parameter of the dependence of the L-shell source field line shift. Decreasing τ and increasing f_0 could indicate a shift to a lower L-shell, and vice versa.

The repetition period τ decreased together with increasing frequency dispersion slope S within the first three intervals (i – iii) indicating possible inward motion of the EMIC wave sources to lower L-shells. But the repetition period τ increased again in interval iv), and the frequency dispersion slope decreased, preserving the tendency of increasing mean frequency, f_0. Then the inverse outward extension of the equatorial EMIC wave source region could be considered after 1800 UT. The L-region width of the sources should had been broadened so that intensive ground signals could be observed within the extensive region in latitude between Ivalo and Oulu. One can also be considered that the plasma characteristics' conditions of the EMIC wave propagation were conserved in the magnetosphere and the increased mean spectral frequency of EMIC waves was preserved during the observation of the whole final period of the ground event.

During the one-hour slow development (1800 – 1900 UT) the magnetic field intensity at Sodankylä approached normal values (see Fig. 3). The ground signal systematically weakened and disappeared both at Ivalo and Oulu after 1920 UT. One can consider that the EMIC wave spectrum, preserved at higher frequencies, did not match the IAR fundamental frequency window when the IAR plasma conditions above the point of

observation reverted to normal. The Pc1 signal on the ground then had to disappear quickly. Later we will demonstrate the relation between the EMIC wave mean frequency variation and variation of the IAR response at the fundamental frequency peak, forming the signal frequency window on the ground.

3. METHOD OF IAR NUMERICAL SIMULATION

The numerical method of simulating the frequency response of IAR in the ionosphere and on the ground was developed on the basis of the 4×4 transformation matrix method applied to a finely stratified inhomogeneous medium according to *Vagner (1982),* and *Prikner and Vagner (1983, 1991).* The inhomogeneous and anisotropic (magnetoactive) medium of the ionosphere has been modelled as finely plane-stratified with external dipole magnetic field $\boldsymbol{B}_0$. Generally the homogeneous plane wave mode of frequency f with wave vector $\boldsymbol{k}$ is assumed to be incident at the ionospheric transition layer (under different local angles $\boldsymbol{k} \wedge \boldsymbol{B}_0$) and propagating to the ground across the elementary homogeneous thin layers coupled with boundary conditions.

The input characteristics of the ionosphere model are the realistic altitude profiles of the electron density, $N_e(z)$, mass of the effective ion in the plasma composition, and profiles of effective ion and electron collisions (electron ↔ ion, and electron and ion with neutrals). Also see eq. (3 – 11) below and Figs 5 – 6.

The general output characteristics are *the complex amplitudes* of the total wave field ($\boldsymbol{B}$, $\boldsymbol{E}$) at an arbitrary altitude level inside the ionospheric transition layer, at its upper boundary, and on the ground surface. The various *real wave characteristics* can be defined and determined on the basis of the complex amplitudes, e.g., transmission and reflection coefficients, Cartesian components of normalized total amplitudes of both the fields everywhere within the ionosphere, or different polarization characteristics as, e.g., in *Prikner et al. (2000).*

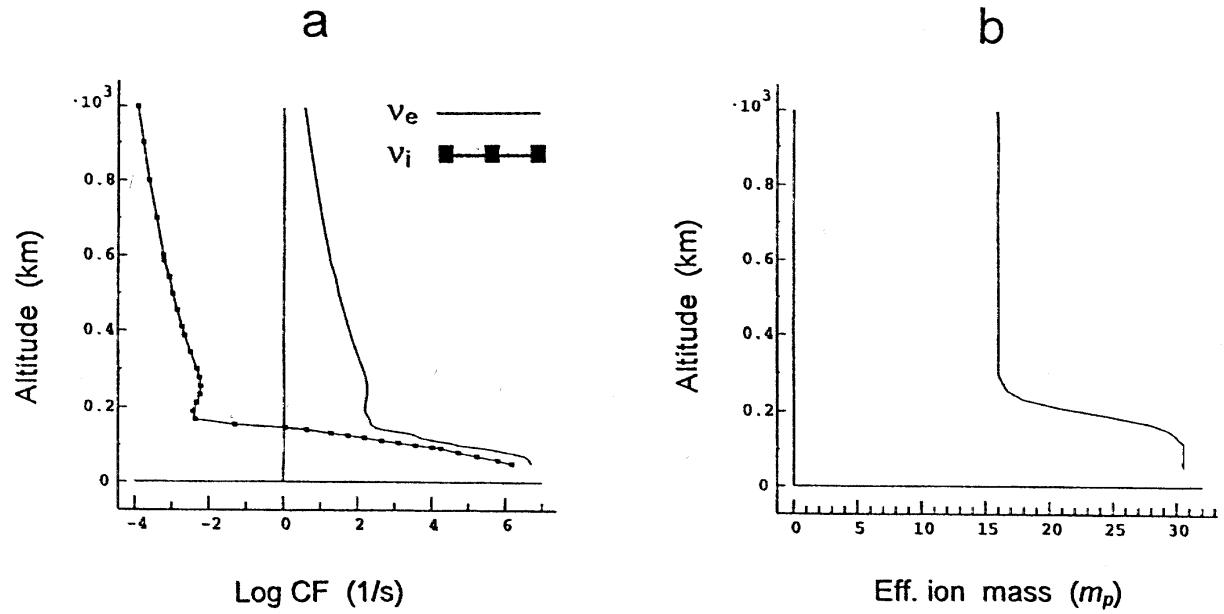

Fig. 5. Examples of the altitude profiles of electron (the smooth curve) and ion (the marked curve) collision frequencies (**a**), and the effective ion mass in proton mass units (**b**), applied to the IAR modelling. These profiles were computed for the 1630 UT point in time.

The normalized real amplitudes of the wave magnetic field in the arbitrary z-altitude layer and at frequency f are treated here in the form

$$NA_{h,v}(f, z) = B_{h,v}(f, z)/B_{h,v}^{inc}(f, z_{max}) , \quad (1)$$

where h and v represent the horizontal and vertical real amplitude, respectively, index "*inc*" indicates the wave incident at the upper ionosphere boundary at $z = z_{max}$. The incident wave can be defined with L- or R-polarization. The L-wave in the Northern Hemisphere is a counterclockwise polarized ordinary Alfvén wave, when viewed along the $\boldsymbol{B}_0$ field line, the R-wave is a clockwise polarized isotropic magnetosonic wave.

The normalized amplitude (1) transforms into *the amplitude transmission coefficient* for a wave with frequency f on the ground surface $z = 0$, defined on the basis of real horizontal B-wave field amplitudes,

$$TA_h(f) = B_h(f, z = 0)/B_h^{inc}(f, z_{max}) . \quad (2)$$

The angle between $\boldsymbol{k}$ and $\boldsymbol{B}_0$ (in the $\boldsymbol{B}_0$ meridional plane) represents different angles of incidence β with respect to the horizontal plane. E.g., $\beta_{||}$ indicates incidence with $\boldsymbol{k} \,||\, \boldsymbol{B}_0(z_{max})$ at the ionosphere boundary $z = z_{max}$.

The numerical simulation method utilizes altitude profiles of the electron concentration N_e, the effective mass of ions in medium M_i, and electron and ion effective collision frequencies ν_e and ν_i under the assumption that the main ionospheric ULF resonator covers a layer of thickness ~1000 km (where the significant N_e can be found).

According to EISCAT data measurements of $N_e(z)$, $T_e(z)$ and $T_i(z)$ (at altitudes $z < 600$ km) the prevailing $NO^+ + O_2^+$ content has been considered at $z < 150$ km. The O^+ content starts to prevail at higher altitudes. At altitudes $z \approx 600 - 1000$ km a moderate change from prevailing O^+ to H^+ can be expected, especially at night and in winter-type models (*Krinberg and Taschilin, 1984; Prikner et al., 2000*). For the purpose of resonator modelling, the $M_i(z)$-profile used for the event examined here is demonstrated in Fig. 5b. It corresponds to high latitudes ($L \approx 5$) in the summer-type ionosphere under disturbed conditions, according to *Krinberg and Taschilin (1984)*.

In conformity with *Fatkullin et al. (1981)* and on the basis of the EISCAT measurements, the altitude profiles of ν_e and ν_i were constructed with regard to the ion-species content in the medium. After *Prikner (1986)*, the formulae containing terms with the T_i quantities were neglected here because their contribution was less by almost one order of magnitude in comparison with the terms of the T_e quantities.

Then at any height the local values are

$$\nu_e = \nu_{en} + \nu_{ei} , \quad (3)$$

$$\nu_{ei} \approx 54 \times 10^{-6} N_e/T_e^{3/2} , \quad (4)$$

where $\nu_{en} \neq 0$ at $z < 150$ km, and $\nu_e \approx \nu_{ei}$ at ≥ 200 km.

$$\nu_i = \nu_{in} + \nu_{ie} , \quad (5)$$

where the data from the EISCAT databank were used for ν_{in} at $z \leq 130$ km. Ion-ion collisions (ν_{ii}) were not considered, since they do not play a part in wave dissipation. Also at $z > 600$ km $\nu_{in} \approx 0$.

$$\nu_{ie} \approx [(\nu \times N)_{NO^+O_{2^+}} + (\nu \times N)_{O^+}]/N_e \qquad \text{(at } z \leq 200 \text{ km)}, \tag{6}$$

$$\nu_{ie} \approx [(\nu \times N)_{O^+} + (\nu \times N)_{H^+}]/N_e \approx \nu_i \qquad \text{(at } z > 600 \text{ km)}. \tag{7}$$

The indices on the r.h.s. of eqs (6 – 7) indicate particular ion species, and

$$\nu_{NO^+O_{2^+}} \approx 9.45 \times 10^{-10}\, N_e/T_e^{3/2}, \tag{8}$$

$$\nu_{O^+} \approx 1.84 \times 10^{-9}\, N_e/T_e^{3/2}, \tag{9}$$

$$\nu_{H^+} \approx 2.94 \times 10^{-8}\, N_e/T_e^{3/2}, \tag{10}$$

where concentration N_e is expressed in m^{-3} and T_e in degrees Kelvin (K).

The altitude profile $M_i(z)$ in proton mass units m_p can be expressed at the arbitrary height level z using local values (Fig. 5b),

$$M_i \approx (30.5\, N_{NO^+O_{2^+}} + 16\, N_{O^+} + N_{H^+})/N_e. \tag{11}$$

To construct the altitude profiles of ν_e, ν_i, the smoothing of values has been applied throughout the transient altitude regions. Nevertheless, testing showed that the positions of the resonant peaks in the frequency spectra slightly depend on the practical variations of the ν-profiles, and the $N_e(z)$-profile remains the principal controlling variable of the resonator with respect to the fundamental frequency response. Examples of the ν_e- and ν_i-altitude profiles (eqs 3, 5) used for modelling in the selected pulsation time 1630 UT and computed on the basis of the EISCAT plasma data are displayed in Fig. 5a.

4. APPLICATIONS

Taking into account the IAR mechanism of Pc1 signal formation on the ground and in the ionosphere, *Prikner et al. (2000)* showed that the $L_{\|}$-wave generated by incidence of the L-wave mode with $\boldsymbol{k} \,\|\, \boldsymbol{B}_0$ conforms well to the IAR wave and plasma altitude profile modelling. The IAR was represented by the main lower 1000 km thick part of the ionosphere (higher low-electron-density layers contribute only a little to the variation of resonator characteristcs mainly at higher harmonics).

The EISCAT incoherent scatter radar in the CP-1 programme scanned the high-latitude ionosphere (geogr. lat. ~69.6°N) up to an altitude of 600 km in the region of Tromsö, which differs in longitude from Ivalo by about 8° to the west. But the very near similar latitudes of both the regions allow the EISCAT data to be combined with IAR modelling above the Ivalo station, where also the intensive pulsation event was recorded.

In the Ivalo region inclination $\boldsymbol{B}_0$ is about −78°. The angle of the $L_{\|}$ – wave mode incidence can then be taken to be $\beta_{\|} = 78°$ with respect to the horizontal plane boundary of the ionosphere at altitude $z = z_{max} = 1000$ km. The Earth's magnetic field dipole moment, $M_E = 8.17 \times 10^{22}$ Am^2, the Earth's surface specific conductivity, $\sigma_E = 10^{-2}$ Sm^{-1}, and the altitude stratification of the ionosphere model, 10 km, were assumed.

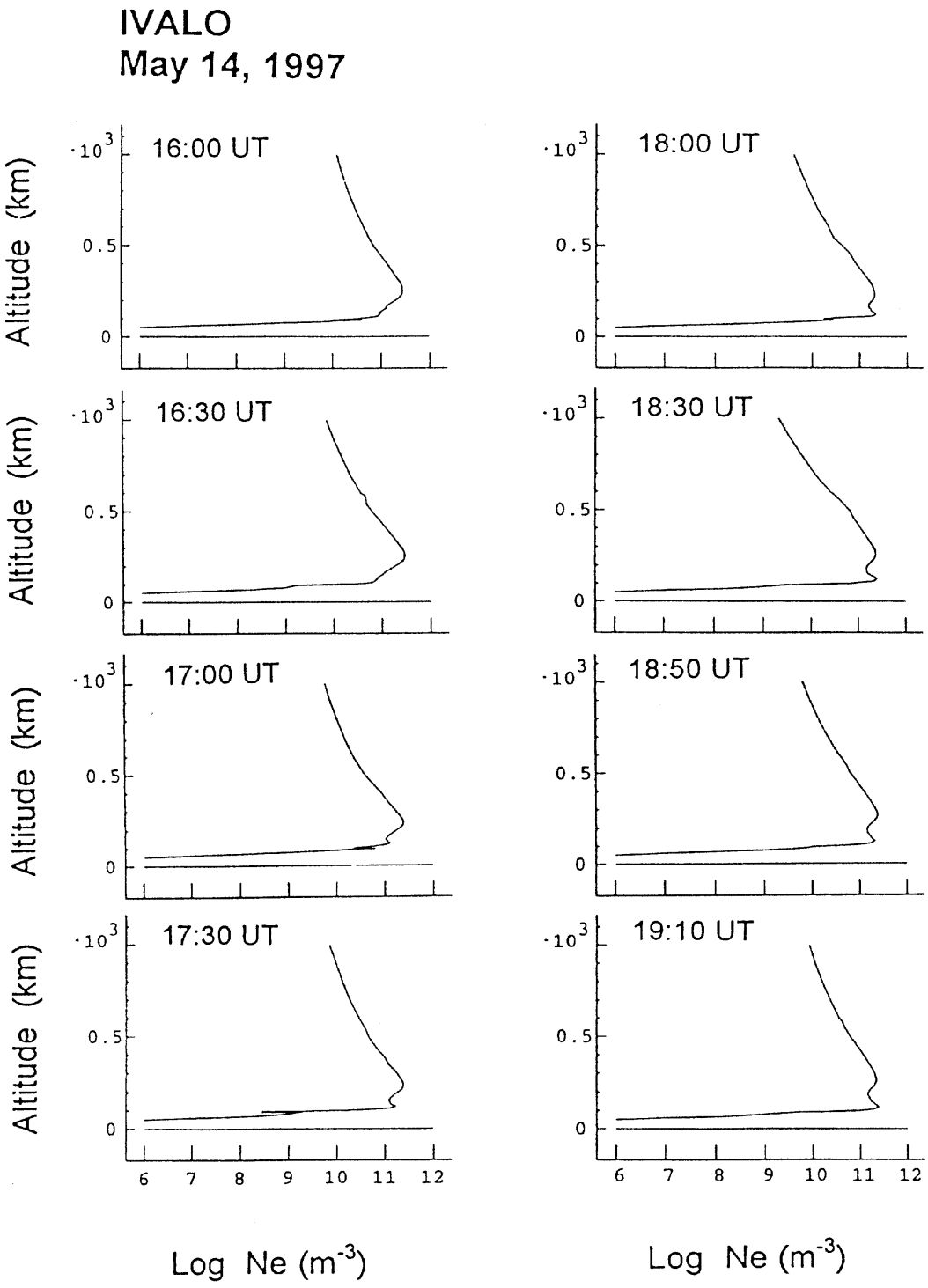

Fig. 6. The eight selected examples of the time variation of the N_e altitude profiles during the Pc1 event, modelled for the Ivalo region on the basis of the EISCAT plasma data given up to 600 km.

The 1000 km thick ionospheric transition layer is the main region determining the IAR fundamental frequency (*Prikner et al., 2000*). Computations of the transmission coefficient (eq. 2) in a broad frequency spectrum can thus illustrate the frequency – time variation of the Pc1 event recorded at Ivalo, using the above mentioned EISCAT plasma profiles, with high accuracy. Computations at 29 points in time during the time interval 1600 – 1910 UT were carried out.

In Fig. 6 eight examples of the N_e-altitude profiles based on the EISCAT data (up to 600 km) are modelled for the Ivalo region providing an image of the local ionosphere N_e-variation during the event. The smooth slopes of the $N_e(z)$ exponential decrease above the F-layer maximum up to 600 km allowed smooth exponential extrapolation of $N_e(z)$ up to $z_{max} = 1000$ km with a constant exponential scale factor. The slow increase of the central frequency (see Fig. 1, 3 – 4) required a slow decrease of N_e at higher altitudes above the F-layer maximum, accompanied by a distinct increase of N_e in the lower E – F1 region.

Examples of transmission coefficient (eq. 2) computations using the IAR N_e-profiles from Fig. 6 and other EISCAT plasma characteristics for determining the resulting ν_e- and ν_i-profiles are shown in Fig. 7. There $L_{||}$-wave transmission through IAR is assumed. The frequency band limits (the width of the real frequency window) of the signal on the Ivalo H-record are marked on the TA_h spectral curves. It can be distinctly seen that the pulsation signal on the ground appears on the record when the fundamental frequency spectral peak matches the EMIC wave spectral frequency band (from about 1600 UT). The intensive and continuous long-lasting pulsation develops when the EMIC wave spectrum entirely merges with the IAR fundamental frequency peak (1630 – 1830 UT), and the IAR fundamental frequency response window is then opened to signals propagating towards the ground. On the contrary the pulsation on the ground weakens and gradually vanishes, when the EMIC wave spectrum misses the IAR fundamental frequency window (between 1845 – 1910 UT).

The process of appearance and disappearance of the signal on the ground is more objectively shown in Fig. 8 for the Ivalo region, including the results of all the 29 transmission coefficient (eq. 2) computations. Moreover, also the results computed for the magnetosonic $R_{||}$-wave transmitting IAR with $\boldsymbol{k} \parallel \boldsymbol{B}_0$ at $z = z_{max} = 1000$ km are given. The control role of the L-wave mode incident at and transmitting through IAR is distinctly shown within the Ivalo signal spectrum limits in Fig. 8. There the central frequencies of the $L_{||}$-wave transmission coefficient peak follow the centres of the pulsation frequency band (after the Ivalo dynamic spectra in Fig. 1).

A tendency for the IAR to recover its initial quiet condition appears at the Ivalo latitude around 1830 UT. The IAR fundamental frequency markedly decreased, but the central frequency of the magnetospheric EMIC wave band evidently remained high. The EMIC wave spectrum missed the IAR fundamental frequency window (see also Fig. 7, after 1850 UT). This led to a rapid weakening and later extinction of the ground signal record between 1845 – 1915 UT. A similar ionosphere – magnetosphere effect evidently also affected the Oulu region (compare Fig. 1 and 8).

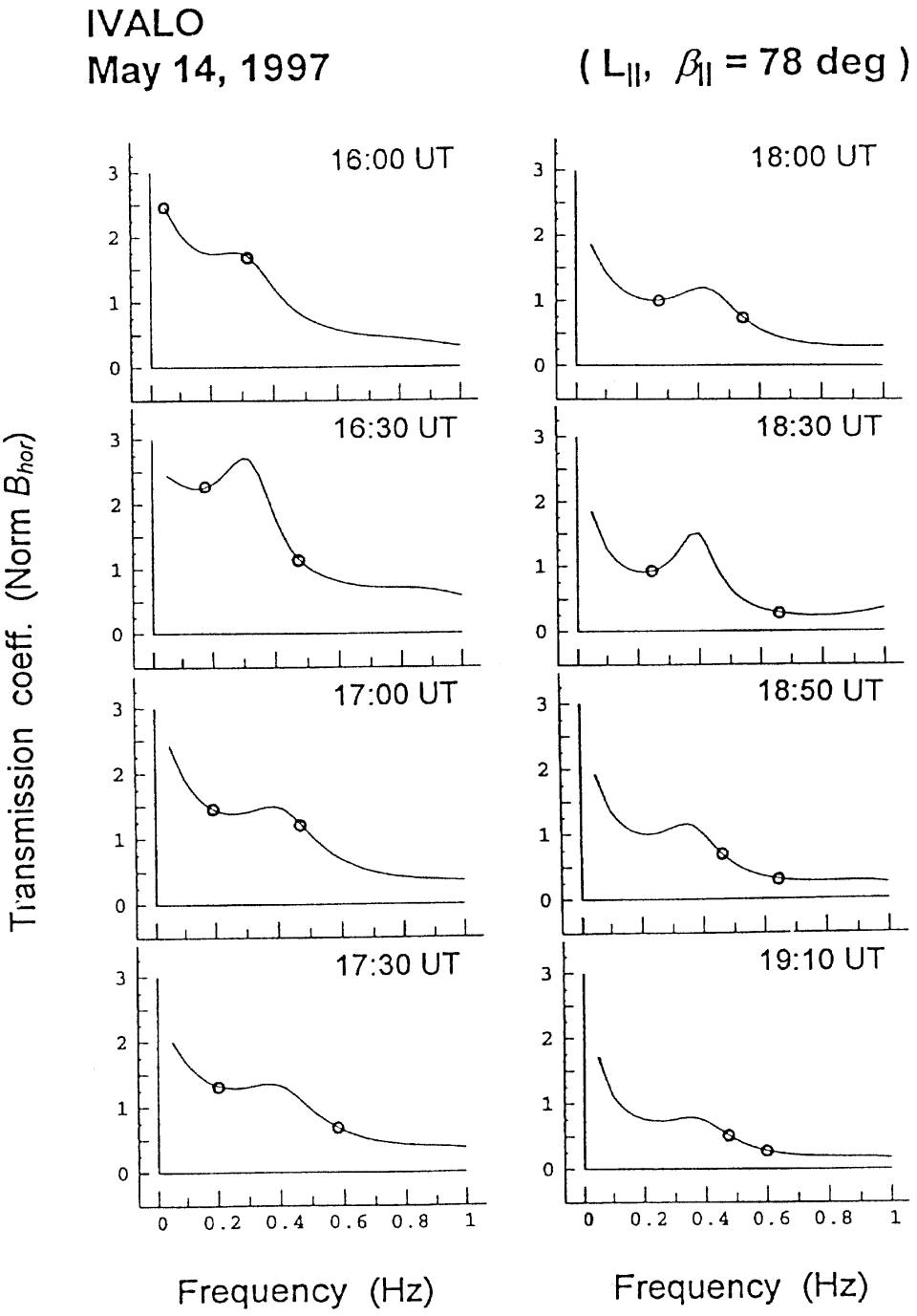

Fig. 7. The time variation of the magnetic field amplitude transmission coefficient modelled for the propagating $L_{||}$-Alfvén wave in the Ivalo region (incidence under angle $\beta_{||} = 78°$ at $z = 1000$ km). The IAR profiles were used for the same times as in Fig. 6. The boundaries of the ground signal frequency windows are demarcated by circles.

5. THE IAR VERTICAL PROFILE OF MAGNETIC FIELD AMPLITUDE AT THE FUNDAMENTAL RESONANCE FREQUENCY

Two points in time were selected to illustrate the variation of the IAR vertical profile of the $L_{||}$- and $R_{||}$-wave magnetic field amplitude at fundamental resonance frequencies in the Ivalo region. At 1630 UT, under initial IAR conditions, the fundamental resonance peak of the $L_{||}$-wave generated by the incidence under angle $\beta_{||} = 78°$ centered at frequency 0.3 Hz, and of the $R_{||}$-wave at frequency 0.4 Hz. Under final IAR conditions at 1830 UT, the fundamental resonance for the $L_{||}$-wave centered at frequency 0.4 Hz and for the $R_{||}$-wave at 0.45 Hz (see also Fig. 8). The *B*-field fundamental resonance was studied separately in the two components – normalized horizontal B_{hor}, and vertical B_{vert} (eq. 1).

The vertical profiles of the normalized B_{hor} amplitude (a, c) and normalized B_{vert} amplitude (b, d) on a logarithmic scale are depicted for both the above mentioned $L_{||}$- and $R_{||}$-waves in Fig. 9. The maximum B_{hor} fundamental resonance amplification (the standing wave antinode) was found within the 150 – 200 km altitude levels in both the points in time, i.e. at the bottom of the F-layer maximum (Figs 9a,c). The B_{hor} fundamental resonance amplification continuously decreased with increasing altitude, its standing wave node being located far above the dense ionosphere. The width of amplification region reached 700 – 800 km. There is the main resonator domain in the fundamental resonance frequency. An antinode in the B_{hor} amplitude locates inside the ionospheric F-layer (horizontal waveguide region according to *Lysak, 1999*).

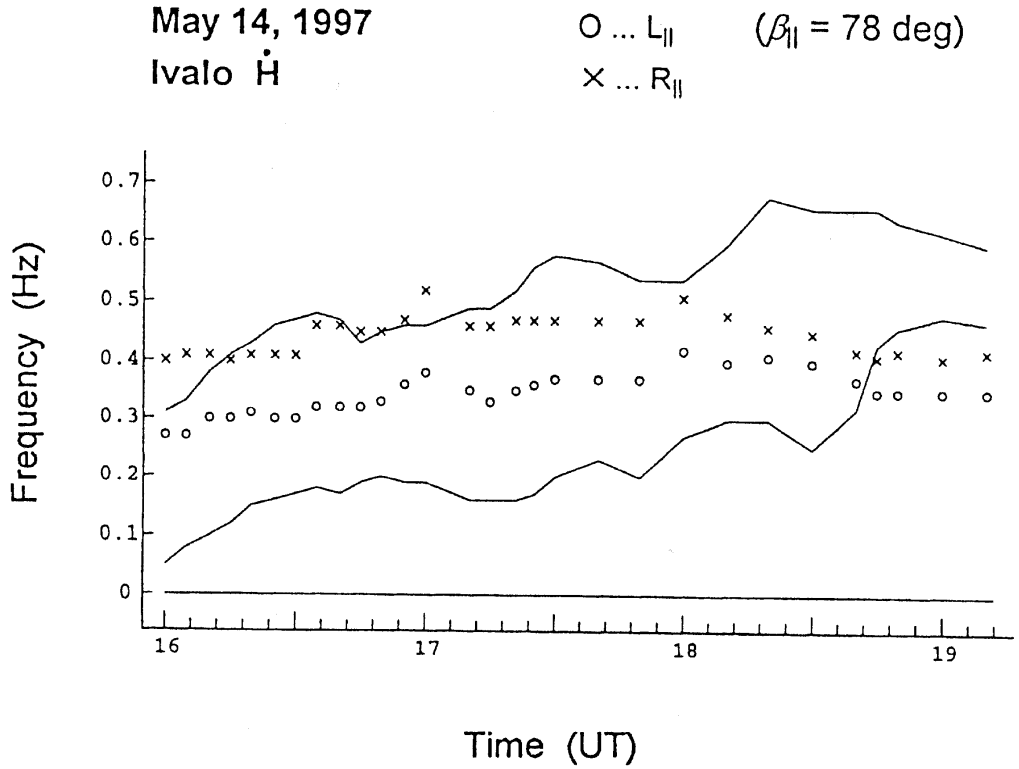

Fig. 8. The time variation of the ground signal frequency window at Ivalo (the H-component, smooth curves) in comparison with the central frequencies of the modelled IAR fundamental frequency peaks of $L_{||}$- and $R_{||}$-waves on the ground.

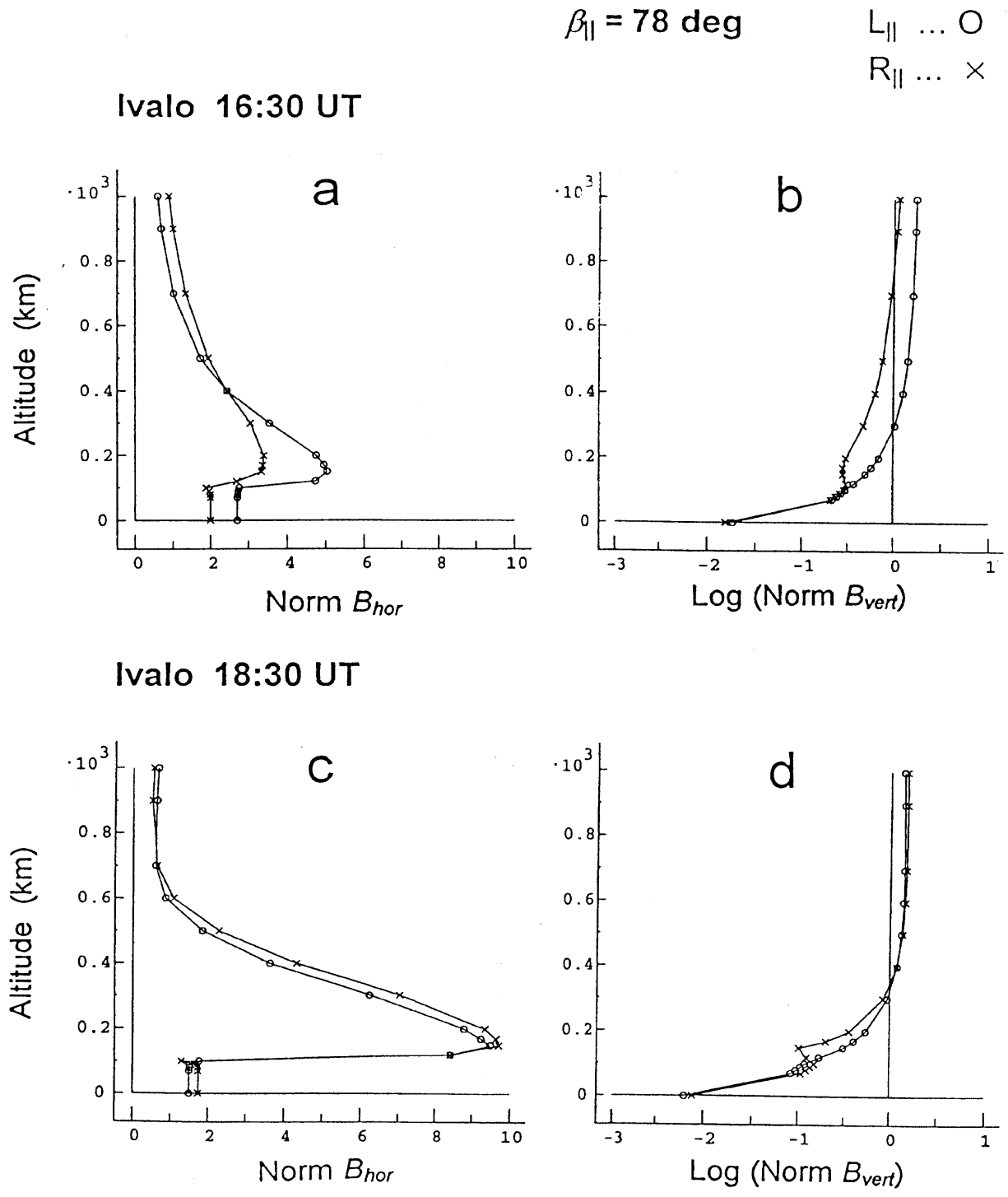

Fig. 9. The altitude profiles of normalized B_{hor} (**a**, **c**) and B_{vert} (**b**, **d** – on a logarithmic scale) modelled at the selected two points in time for the Ivalo region and both the $L_{||}$- and $R_{||}$-waves at the fundamental resonances. At 1630 UT: $f_{res}{}^{L} = 0.3$ Hz and $f_{res}{}^{R} = 0.4$ Hz; at 1830 UT: $f_{res}{}^{L} = 0.4$ Hz and $f_{res}{}^{R} = 0.45$ Hz (see also Fig. 8).

There is not the first-hand analogy with the simple model of standing wave generation in *Jordan and Balmain (1968)* (the vacuum medium and perfect conductivity of the Earth's surface). Within the realistic inhomogeneous ionosphere the standing wave structure presents as an altitude-sliding phenomenon in dependence on the $N_e(z)$-profile variation. The shear Alfvén wave resonance producing compressional modes can be transported into the horizontal waveguide, if the resonant frequency matches the first harmonic resonance of the waveguide (*Lysak, 1999*).

From Fig. 9c (1830 UT) it is evident that the B_{hor} amplification was sharper and the width of the amplification region became smaller towards the lower altitudes (< 600 km) in comparison with the 1630 UT time in Fig. 9a. It indicates decreasing effective dimensions of IAR during the pulsation event examined. The B_{hor} fundamental resonance amplification near the value of 2 was found below the ionosphere and on the ground surface. It agrees with the simple model of wave reflection at the boundary with high conductivity as in *Jordan and Balmain (1968)*.

The normalized B_{vert} amplitude profiles in Fig. 9b, d, show the standing wave node at the fundamental B_{vert} resonance at the bottom of the ionosphere and on the ground, and the antinode far above the dense ionosphere. Comparing the normalized B_{hor} and B_{vert} profiles, it is evident that the IAR resonance maximum amplification has been found mainly in the horizontal magnetic field component B_{hor} quite below the ionospheric F-layer maximum. The maximum amplification there was as much as ten times higher than the amplitude of the incident wave at $z_{max} = 1000$ km.

No fundamental differences were found between the $L_{||}$- and $R_{||}$-wave B-amplitude profiles. However, Figs 9b,c,d show the lower normalized B_{vert} and greater B_{hor} amplitudes for the $R_{||}$-wave as compared to the $L_{||}$-wave especially within the dense F-layer ionosphere. The $R_{||}$-wave is a resultant *isotropical* wave. On the other hand, the $L_{||}$-wave is well guided along the external magnetic field lines. It accounts for the differences between the both resonance frequencies.

6. DISCUSSION

The analysed Pc1 event of May 14, 1997, recorded at the chain of Finnish observatories, was one of the rare long-term events with simultaneous EISCAT measurements providing plasma profiles over a wide altitude extent up to 600 km. The EISCAT measurements were performed at latitudes close to the latitude of the signal observation point. The time variation of the dynamic pulsation spectra can then be well correlated with the variation of the IAR fundamental frequency response modelled on the basis of varying real EISCAT ionosphere plasma characteristics.

An analytical extension of the plasma profiles at altitudes between 600 – 1000 km with the electron density decreasing exponentially was possible and appropriate small deviations in its scale factor could not affect the IAR fundamental frequency value much. The Alfvén $L_{||}$-wave fundamental resonance peaks followed the variation of the frequency band of the signal dynamic spectra exactly within the interval of the well-developed ground Pc1 event.

The initial part of the ground Pc1 record with the clearly defined frequency band appeared around 1610 UT, when the EMIC wave spectrum matched the well-developed IAR fundamental frequency peak. On the contrary, the ground signal dimmed after

1900 UT and finally disappeared when the EMIC wave frequency spectrum and the IAR fundamental frequency peak began to differ. Especially the combination of these initial and final effects supports the idea of IAR control mechanism of Pc1 and IPDP signals within the ionosphere and on the ground.

The IAR f_0-antinode in the horizontal magnetic field amplitude is located within the F-ionosphere region both for the L- or R-wave types. The Alfvén $L_{||}$-wave with parallel incidence $\boldsymbol{k} \parallel \boldsymbol{B}_0$ represents the center of the possible incident $\boldsymbol{k}$-wave beam (assumed $\boldsymbol{k}$-fan bunch in the meridional plane), generating the Pc1 signal as a multiple-wave response of IAR in the fundamental frequency window within the ionosphere and on the ground. Continuously variable effective dimensions of IAR are specified mainly by the vertical profile of the plasma composition (i.e. electron density profile). The nonstationary plasma composition along the vertical gives rise to the frequency variable Pc1, as well as the IPDP types of pulsations in high-latitude substorms in dependence on the movable IAR fundamental frequency spectral window.

7. CONCLUSION

A slow shift of the EMIC-wave source to lower L-shells during the event was established by studying the signal pearl structure. The disturbance source field lines gradually shifted to lower latitudes from the Ivalo to the Oulu region at about 1730 UT. After 1800 UT an indication of the tendency for the outward shift of the EMIC-wave source L-shell to recover was observed (changes in parameter τ/f_0 according to *Mursula et al., 1999b*). These variations were followed by the variations of the IAR frequency characteristics.

The applied numerical method of ionospheric wave filtration is able to illustrate the variation of the IAR fundamental frequency window. The comparison between the ground-observed dynamic characteristics of the signal and the simulated variation of the IAR frequency window (based on the EISCAT data) was able indicate the times of the beginning and extinction of the ground-observed signal (the control effect). The discrepancy between the magnetospheric EMIC-wave frequencies and the IAR fundamental frequency window (during the ionosphere recovery, if any, after 1850 UT at higher latitudes) led to the dimming and disappearance of the signal on the ground record after 1915 UT (see Figs 1 and 8). Then we can anticipate the IAR control mechanism on the signal transmitting to the ground.

Acknowledgements. K. M., J. K., and T. P. gratefully acknowledge the financial support of the Academy of Finland. F. Z. F. gratefully acknowledges the financial support of the Commission of the European Union (Brussels) through Research Grant INTAS 99-0335. K. P. thanks T. Pikkarainen for the magnetic data and P. Pollari for the EISCAT data.

The EISCAT Scientific Association is supported by the Suomen Akatemia of Finland, Centre National de la Recherche Scientifique, France, Max-Planck Gesellschaft, Federal Republic of Germany, National Institute of Polar Research of Japan, Norges Almenvitenskapelige Forskningsrad of Norway, Naturvetenskapliga Forskningsradet of Sweden, and the Science and Engineering Research Council of the United Kingdom.

Manuscript received: 11 April 2001; Revisions accepted: 14 June 2001

References

Altman C. and Fijalkow E., 1980. The horizontal propagation of Pc1 pulsations in the ionosphere. *Planet. Space Sci.*, **28,** 61-68.

Bauske R., Noel S. and Prölss G.W., 1997. Ionospheric storm effects in the nighttime E region caused by neutralized ring current particles. *Ann. Geophysicae,* **15,** 300-305.

Belyaev P.P., Polyakov S.V., Rapoport V.O. and Trakhtengerts V. Y., 1990. The ionospheric Alfvén resonator. *J. Atmos. Terr. Phys.,* **52,** 781-788.

Demekhov A.G., Trakhtengerts V.Y. and Bösinger T., 2000. Pc1 waves and ionospheric Alfvén resonator: generation or filtration? *Geophys. Res. Lett.,* **27** (No.23), 3805-3808.

Demekhov A.G., Trakhtengerts V.Y., Polyakov S.V., Belyaev P.P. and Rapoport V.O., 1994. An Alfvén sweep maser model for Pc1 pearls: Theory. In: *NIRFI's preprints,* pp. 1-26, NIRFI, Nizhny Novgorod, Russia.

Erlandson R.E., Anderson B.J. and Zanetti L.J., 1992. Viking magnetic and electric field observations of periodic Pc1 waves: pearl pulsations. *J. Geophys. Res.,* **97,** 14823-14832.

Erlandson R.E., Mursula K. and Bösinger T., 1996. Simultaneous ground – satellite observations of structured Pc1 pulsations. *J. Geophys. Res.,* **101,** 27149-27156.

Fatkullin M.N., Zelenova T.I., Kozlov V.K., Legenka A.D. and Soboleva T.N., 1981. Empirical models of the mid-latitude ionosphere (in Russian). Nauka, Moscow.

Fraser B.J., Singer H.J., Hughes W.J., Wygant J.R., Anderson R.R. and Hu Y.D., 1996. CRRES Poynting vector observations of electromagnetic ion cyclotron waves near the plasmapause. *J. Geophys. Res.,* **101,** 15331-15343.

Fujita S., 1987. Duct propagation of a short-period hydromagnetic wave based on the international reference ionosphere model. *Planet. Space Sci.,* **35,** 91-103.

Greifinger C. and Greifinger P.S., 1968. Theory of hydromagnetic propagation in the ionospheric wave guide. *J. Geophys. Res.,* **73,** 7473-7490.

Jacobs J.A. and Watanabe T., 1964. Micropulsation whistlers. *J. Atmos. Terr. Phys.,* **26,** 825-829.

Jordan E.C. and Balmain K.G., 1968. Electromagnetic waves and radiating systems. Prentice – Hall, Inc., Englewood Cliffs, New Jersey.

Kleimenova N.G., Kangas J., Pikkarainen T. and Ranta C., 1995. The geomagnetic pulsations IPDP and the main ionospheric trough (in Russian). *Geomag. Aeron.,* **35,** 60-68 (Russian edition).

Krinberg I.A. and Taschilin A.V., 1984. The ionosphere and the plasmasphere (in Russian). Nauka, Moscow.

Lysak R.L., 1991. Feedback instability of the ionospheric resonant cavity. *J. Geophys. Res.,* **96,** 1553-1568.

Lysak R.L., 1993. Generalized model of the ionospheric Alfvén resonator. In: *Auroral Plasma Dynamics, Geophysical Monograph,* **80,** American Geophysical Union, 121-128.

Lysak R.L., 1999. Propagation of Alfvén waves through the ionosphere: Dependence on ionospheric parameters. *J. Geophys. Res.,* **104** (A5), 10017-10030.

Mursula K., Bräysy T., Rasinkangas R., Taskanen P. and Mozer F., 1999a. A modulated multiband Pc1 event observed by Polar/EFI around the plasmapause. *Adv. Space Res.*, **24**(1), 81-84.

Mursula K., Kangas J., Kerttula R., Pikkarainen T., Gugliel'mi A., Pokhotelov O. and Potapov A., 1999b. New constraints on theories of Pc1 pearl formation. *J. Geophys. Res.*, 104 (A6), 12399-12406.

Mursula K., Prikner K., Feygin F.Z., Bräysy T., Kangas J., Kerttula R., Pollari P., Pikkarainen T. and Pokhotelov O.A., 2000. Non-stationary Alfvén resonator: new results on Pc1 pearls and IPDP events. *J. Atmos. Sol.-Terr. Phys.*, 62, 299-309.

Mursula K., Rasinkangas R., Bösinger T., Erlandson R.E. and Lindqvist P.-A., 1997. Nonbouncing Pc1 wave bursts. *J. Geophys. Res.*, 102, 17611-17624.

Obayashi T., 1965. Hydromagnetic whistlers. *J. Geophys. Res.*, **70,** 1069-1087.

Polyakov S.V., 1976. On properties of an ionospheric Alfvén resonator. In: *Symposium KAPG on Solar - Terrestrial Physics,* Vol. III, pp. 72-73. Nauka, Moscow.

Polyakov S.V. and Rapoport V.O., 1981. Ionospheric Alfvén resonator. *Geomag. Aeron.*, **21,** 610-614.

Prikner K., 1986. The ionosphere of higher geomagnetic latitudes ($L = 3$ and $L = 5$) as a ULF wave filter. *Studia geoph. et geod.*, **30,** 304-319.

Prikner K., Mursula K., Feygin F.Z., Kangas J., Kerttula R., Pikkarainen T., Pokhotelov O.A. and Vagner V., 2000. Non-stationary Alfvén resonator: vertical profiles of wave characteristics. *J. Atmos. Sol.-Terr. Phys.*, **62,** 311-322.

Prikner K. and Vagner V., 1983. Numerical modelling of the ionospheric filtration of an ULF micropulsation signal. *Studia geoph. et geod.*, **27,** 173-190.

Prikner K. and Vagner V., 1991. Numerical solution to the problem of ionospheric filtration of ULF waves in the Pc1 range. The total wave field inside the ionospheric transition layer. *Studia geoph. et geod.*, **35,** 90-99.

Rasinkangas R. and Mursula K., 1998. Modulation of magnetospheric EMIC waves by Pc3 pulsations of upstream origin. *Geophys. Res. Lett.*, **25,** 869-872.

Trakhtengerts V.Y., Demekhov A.G., Polyakov S.V., Belyaev P.P. and Rapoport V.O., 2000. A mechanism of Pc1 pearl formation based on the Alfvén sweep maser. *J. Atmos. Sol.-Terr. Phys.*, **62,** 231-238.

Vagner V., 1982. Numerical solution of ionospheric filtration of ULF waves (Part 1 – Method). *Travaux Géophysiques,* **XXX** (No 576), 199-229.